Comparison Analysis of Starspots and Historical Sunspot Data

Jack Cousins
Instructor: Dr. P. Kenneth Seidelmann

University of Virginia
Department of Astronomy
May 2024

This thesis is submitted in partial completion
of the requirements of the BA Astronomy Major.

Abstract

Dark regions commonly appearing on the Sun's surface are known as "sunspots." These areas of solar activity are a result of cooled regions of magnetic flux within the Sun's photosphere. Areas of higher solar-magnetic activity heat regions of both the photosphere and chromosphere, leading to a rise in magnetic flux (Φ) to the upper regions of the Sun. The lower, cooler areas of flux within the photosphere are what are ultimately viewed as the dark "sunspots" on the Sun (National Oceanic and Atmospheric Administration, 2024, Ret. April 29, 2024). While the specific heliophysics behind the formation, evolution, and eventual decay of sunspots is not currently fully understood, extensive historical documentation of the number of sunspots present on the Sun exists and dates back to the 18th century (Royal Observatory of Belgium, 2015, Ret. April 29, 2024). Historical sunspot number (SSN) data have been used to assert the cyclic nature of the presence of sunspots on the Sun, similar to the well-understood cyclic nature of the Sun's activity via the 11-year Schwabe Cycle and 90-year Gleissberg Cycle.

Sunspots that occur on stars other than our own Sun are commonly referred to as "starspots." Our current understanding of starspots leads us to believe that they occur and behave similarly to their Sun-counterpart. Their detection and cycle lengths, however, vary greatly from the present methodology of documenting sunspots.

This thesis outlines the similarities and differences between sunspots and detected starspots on stars similar in type to the Sun (Le Mouël, Lopes, & Courtillot, 2020, Ret. April 29, 2024). A comparison analysis of sunspots' and starspots' physical characteristics and detection methodologies is also included. Present-day exoplanet detection often requires the use of these methodologies, leading to a stark overlap in exoplanet and starspot research. This thesis provides additional information on the ongoing dynamic between sunspot research and exoplanet identification. Finally, the comparison of type, detection, and background of sunspots and starspots reveals the presence of other solar activity on stars similar in type to the Sun. Future study through repeated extensive observations will likely be required to make definitive claims about the nature of starspots present on the surface of main sequence stars similar to the Sun. The documented success of present starspot detection methodologies is, however, promising for prospective research on the topic of starspots.

Table of Contents

Introduction

1.1 Sunspots

"Sunspots" are dark, spot-like features that appear in the Sun's photosphere (National Oceanic and Atmospheric Administration, 2024, Ret. April 28, 2024). Based upon their cyclic nature, sunspots are presumed to be a product of the Sun's ever-changing "solar magnetic dynamo." The solar dynamo is not currently fully understood. Current models of its nature agree that the Sun's magnetic field is generated by the movement of ionized gas, specifically plasma (Hathaway, 2023, Ret. April 29, 2024). Often referred to as "the fourth state of matter," plasma occurs as a gas-like flow throughout the Sun's inner layers (Bowman, 2023, Ret. April 29, 2024). Its existence within the Sun is a result of nuclear fusion occurring deep inside the Sun's core. The majority of the Sun's energy output is generated via core nuclear fusion. While this thesis does not specifically address the complexity of solar nuclear fusion, it is important to note its significance in the formation of plasma. Core nuclear fusion releases a considerable amount of energy and heat throughout the inner layers of the Sun (Bolles, 2024, Ret. April 29, 2024) [Core temperatures can reach up to 15 million degrees Fahrenheit, ~8.3 million degrees Celsius (Orr & Espinoza, 2017, Ret. April 29, 2024)]. This energy release sufficiently heats the Sun's inner gasses, causing the separation of negatively charged electrons and positively charged ions to occur within said gasses (Bowman, 2023, Ret. April 29, 2024). The resulting conducting matter is referred to as "plasma" (National Research Council, 2004, Ret. April 29, 2024). Further heating and electrostatic interactions cause plasma to flow throughout the layers of the Sun (Bowman, 2023, Ret. April 29, 2024). Electric charge generated as a result of this moving plasma creates highly dynamic, highly complicated loops of solar magnetic fields. The Sun's rotational mechanics induce a "stretching effect" that elongates these magnetic field loops from pole to pole. Satisfactory "stretching" can cause some loops to rise and break through the superheated surface of the Sun. Areas where these loops have erupted prevent the previously outlined convective cycle of plasma from occurring. These areas are considerably cooler in temperature than places where loops have not broken through. Ultimately, the difference in temperature between these two solar areas is what causes the dark spots we view on the Sun as "sunspots" (Royal Museums Greenwich, 2023, Ret. April 29, 2024; National Oceanic and Atmospheric Administration, 2024, Ret. April 29, 2024).

The total number of sunspots on the Sun's surface at a given time generally aligns with the stage at which the Sun is in its 11-year "solar cycle." Larger and more intense sunspot activity is known to occur during the Sun's "solar maximum," whereas "solar minimum" generally sees a reduction in the amount and strength of sunspots (National Oceanic and Atmospheric Administration, 2024, Ret. April 29, 2024). The Sun is currently in Solar cycle 25 which began in December 2019 and followed Solar cycle 24 [December 2008 - December 2019] (National

Oceanic and Atmospheric Administration Solar Cycle Progression, 2024, Ret. April 29, 2024). Total sunspot number variability during each defined Solar cycle has been well documented, with the total sunspot number (SSN) being accurately maintained on a monthly basis since 1749 and on a daily basis since 1818 (National Centers for Environmental Information, 2016, Ret. April 29, 2024). Similar levels of variability have been observed on solar-type stars as a result of “sunspots" occurring on other stars (Namekata et al., 2019, Ret. April 29, 2024).

Sunspots present several observable characteristics. The “umbra” is the central dark region pictured below. Sunspots initially present themselves strictly as this darker region, with smaller strand-like “penumbrae” regions appearing as the sunspot develops. Spots of less magnetic flux (Φ) intensity are known as “pores.” These features are usually less dense and present cooler temperatures but are known to interact and “clump” together to form more mature umbrae. Although their appearance is small relative to the scale of the Sun, sunspots are oftentimes many magnitudes larger than the Earth, with the densest regions of activity during solar maximum known to cover considerable distances across the Sun (National Oceanic and Atmospheric Administration, 2024, Ret. April 29, 2024).

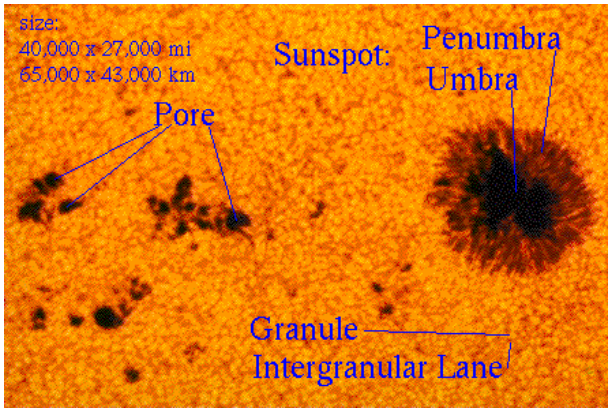

Figure 1: Sunspot diversity and their relative size across the Sun (StarChild | NASA, n.d., Ret. April 29, 2024).

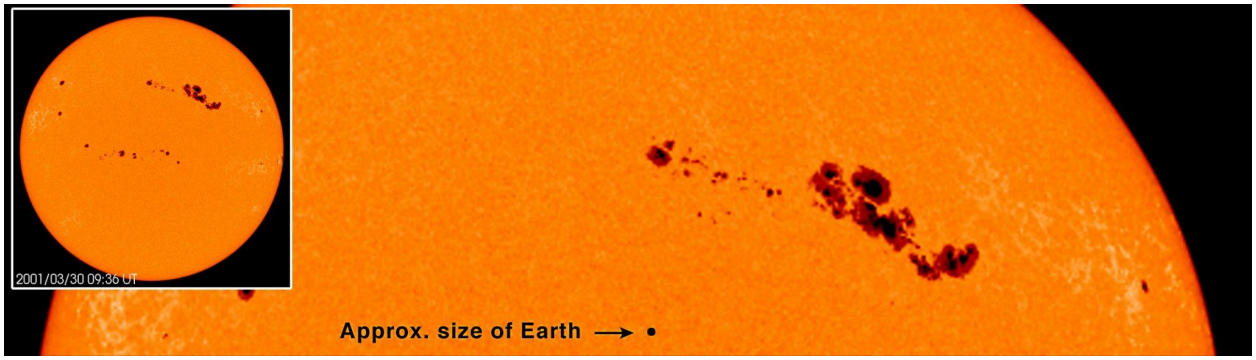

Figure 2: “Active region 9393 as seen by MDI hosted the largest sunspot group observed during solar cycle 23,” with the approximate size of Earth included (Solar and Heliospheric Observatory, 2020, Ret. April 29, 2024). Solar cycle 23 occurred from November 1996 - December 2008 (National Oceanic and Atmospheric Administration Solar Cycle Progression, 2024, Ret. April 29, 2024).

1.2 Sunspot Detection

Sunspots have long been a defining element of solar variability study, with the earliest documentation of sunspot observation occurring as early as the 12th century CE. Early detection of sunspots proved difficult due to the occluding nature of the atmosphere and the overall brightness of the Sun. The development of the modern telescope alongside the invention and development of photography proved to be crucial in garnering today’s more comprehensive understanding of the heliophysical nature of sunspots. A summary of the most historically prominent sunspot detection methodologies can be found below (Arlt & Vaquero, 2020, Ret. April 29, 2024).

Naked-Eye Observation

The earliest, and therefore most basic methodology used for sunspot detection was through “naked-eye” observations. Disregarding the obvious hazard of observing the Sun directly, early naked-eye observations lack the distinct visual and mathematical detail that modern detection tools offer. Pre-telescopic sunspot detections required a specific balance in atmospheric clarity via natural aerosols, including dust, haze, and fog, to make direct observations of the Sun a possibility. The above aerosols served as a natural filter that allowed direct viewing of the Sun, while clouds often blocked an excessive amount of light, ultimately making direct viewing impossible. The sum of these observational requirements is commonly attributed as the main reason for the lack of early graphical/illustrative sunspot observations, with early astronomers favoring written descriptions of detections. This conclusion was the result of several extensive studies occurring in the 20th century, specifically examining early accounts of solar activity from East Asian authors and perspectives. Perhaps the two most significant graphical representations of early sunspot detections are dated as early as 1128 CE and 1424-1425 CE, respectively. The earliest, a simple drawing authored by the chronicler John of Worcester of England, depicts the dark, spotlike nature of sunspots and is currently one of many archives of Corpus Christi College, Oxford (Willis, Wild, & Warburton, 2016, Ret. April 29, 2024). The second, a painted representation of sunspots, is of the Chinese Manuscript *Tı̄anyuán Yùlì Xiángyìfù*, now in the possession of the National Archives of Japan. Both of these early detections of sunspots exemplify the issues of detail and proportion that early astronomers encountered through naked-eye observation (Arlt & Vaquero, 2020, Ret. April 29, 2024).

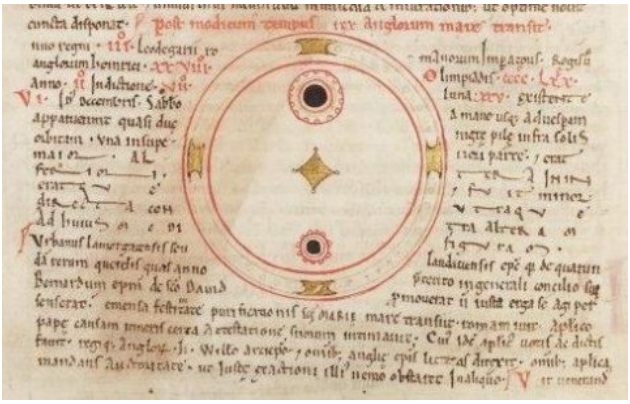

Figure 3: Chronicler John of Worcester's early depiction of sunspots, 1128 CE (Blyth, n.d., Ret. April 29, 2024).

Figure 4: Ti¯anyuán Yùlì Xiángyìfù, manuscript depiction of starspots, compiled 1425-1425 CE (Arlt & Vaquero, 2020, Ret. April 29, 2024).

Early Telescopic Detection

The development of the first astronomical telescopes solved many of the problems early naked-eye observers encountered when attempting to detect and detail sunspots. Early forms of the Galilean and Keplerian telescopes allowed for the projection of the Sun onto a screen. Observers could then easily illustrate sunspots directly on the screen, and then copy their observations onto separate pieces of parchment for further analysis. Although this process presents itself as archaic in modern terms, the accuracy of the historic total sunspot number (SSN) has been maintained using this method to this day (National Centers for Environmental Information, 2016, Ret. April 29, 2024; Tran & Thomas, 2020, Ret. April 29, 2024). As

observational technology improved through the 18th and 20th centuries, astronomers began favoring measuring sunspot locations as opposed to illustrating their appearances. This methodology introduced empirical implications regarding the scale area and transit times of sunspots occurring during this period. The majority of early sunspot measurements were not drawn to scale and thus lack spot size accuracy and grouping precision. Early sunspot period measurements were initially described in terms of their advancement across the solar disk. This disk was commonly partitioned into six concentric circles that resulted in 12 total “bands” that could be used to depict a particular spot’s course across the Sun [similar to the geographic coordinate system of latitude and longitude of the Earth] (Neuhäuser, Arlt, & Richter, 2018, Ret. April 29, 2024). Accurate solar coordinates of spot transits required an additional directional parameter. This was commonly accomplished by timing spot transits through “crosshair” eye-piece additions, which made use of the fact that “apparent solar rotation is approximately symmetric with respect to a certain line close to the equator.” Early sunspot areas have since been appropriately scaled using modern “binning” methodologies, while sunspot periods have been refined through comparative analysis of sunspot illustrations and measurements occurring on the same or nearby days (Arlt & Vaquero, 2020, Ret. April 29, 2024).

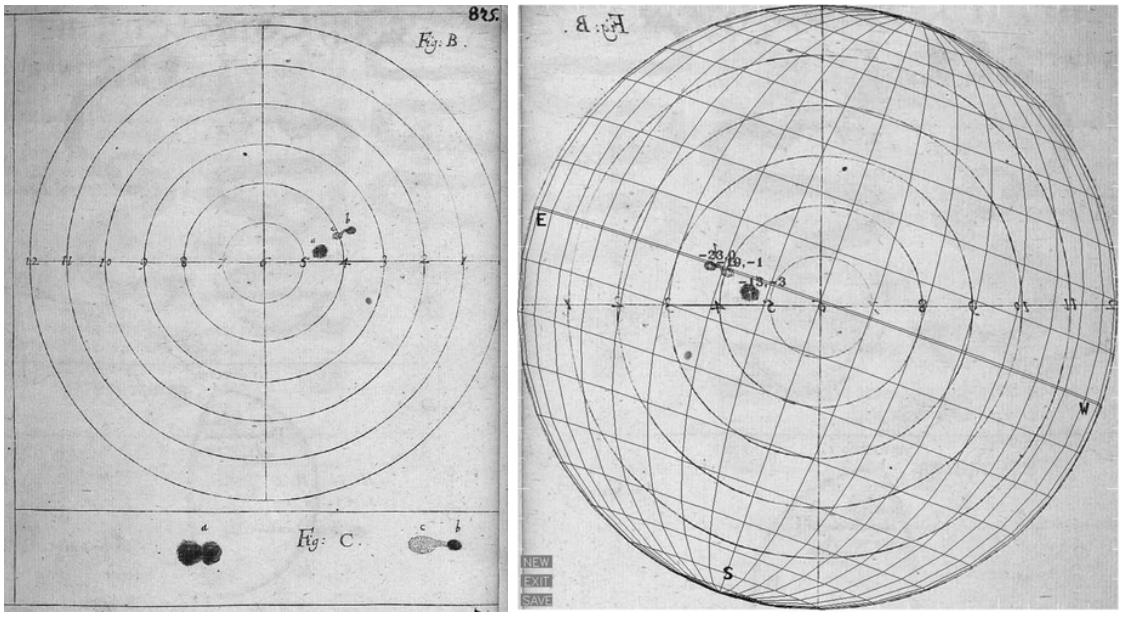

Figure 5: Left; Original sunspot drawing by Kirch on 1680 May 22 (Greg.) as observed with a 10-ft-telescope and using a projection screen. Right; Mirrored version with measured sunspot position (modern adjustment) (Neuhäuser, Arlt, & Richter, 2018, April 29, 2024).

Present Detection and Observational Methodologies

While the historical sunspot number (SSN) continues to be maintained by astronomers globally using the early screen-and-print method, sunspots are primarily detected and documented today by photographic and instrumental means (Tran & Thomas, 2020, Ret. April 29, 2024). Sunspot analysis is regularly performed through data captured by the Solar Dynamics Observatory satellite (SDO). While SDO was originally launched to study general solar variability, its imaging array allows for accurate transit analysis of sunspots in the optical, as well as further evaluation of the solar magnetic dynamo in a multitude of wavelengths (Pesnell & Patel, n.d., Ret. April 29, 2024; Stanford Solar Group, 2010, Ret. April 29, 2024). High-resolution analysis has also taken place through ground-based imaging. The Daniel K. Inouye Solar Telescope (DKIST) of the Haleakala Observatory has produced numerous highly-resolved optical images of sunspots, allowing for further analysis of sunspot development, evolution, and dynamics (U.S. National Science Foundation, n.d., Ret. April 29, 2024). The DKIST's simultaneous use of adaptive and active optics calibrates out the atmospheric seeing effects described above that once plagued naked-eye and early telescopic observations of sunspots (Johansson, n.d., Ret. April 29, 2024). It should be noted that sunspot detection and general solar variability study are not solely compiled by the above satellites and observatories. Understanding the nature of sunspots requires further analysis of the Sun's ever-changing solar magnetic dynamo. Hour-by-hour measurements of the Sun's variability are assembled by solar observatories across the globe. Almost daily research papers are published on the topic of sunspots as a result of this combined global effort to further understand the Sun's historic variation.

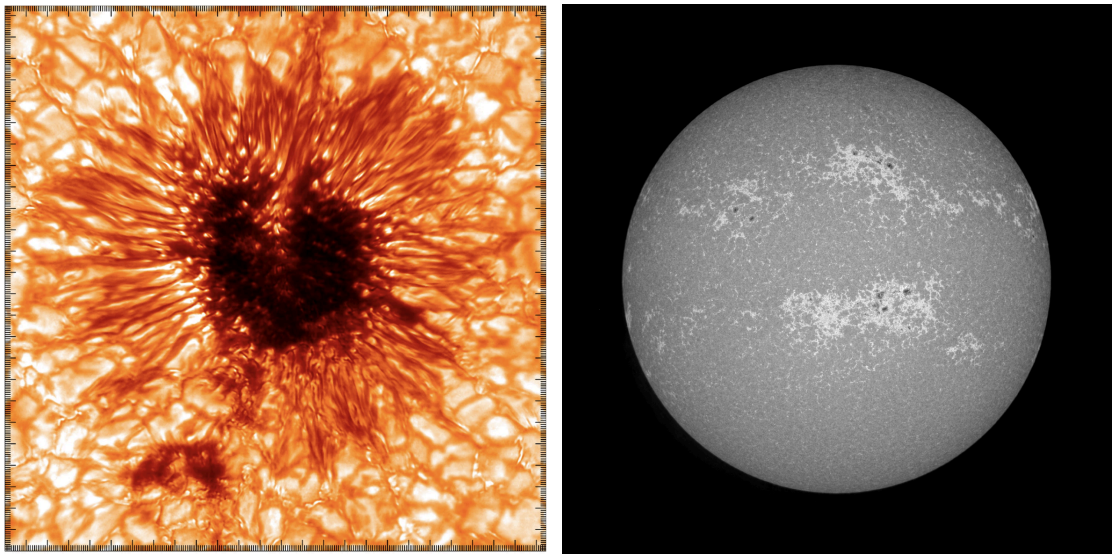

Figure 6: Left; The first sunspot image taken on Jan. 28, 2020, by the NSF's Inouye Solar Telescope's Wave Front Correction context viewer (Rimmele et al., 2020, Ret. April 29, 2024). Right; SDO image of Sun in continuum 1700 Å with several sunspots clearly visible, taken 2024/04/20 17:24:28 UTC (Solar Dynamics Observatory | NASA, 2024, Ret. April 29, 2024).

1.3 Starspots

Similar to sunspots, “starspots” are darker, cooler areas occurring on the surface of stars other than the Sun (Giles et al., 2017, Ret. April 29, 2024). Starspots were long considered as the reason for the stellar and supernova variability of astronomical objects in the night sky. As early as 1667, French astronomer and philosopher Ismaël Bullialdus was credited with accurately defining omicron Ceti’s stellar variability period, while also introducing the first physical model to give reason for stellar variability of variable stars - as a direct consequence of starspots. Furthermore, starspots continued to be used as the basis for stellar variability in newly discovered variable stars of the late 17th, 18th, and 19th centuries. Even astronomical observations as irregular as supernovae explosions were explained by starspot-like activity during the mid-to-late 19th century, with American astronomer William A. Norton noting in 1845 that, “stars in their pre-nova state would have been covered so thickly in dark spots on both hemispheres to be virtually non-luminous.” The application of starspots as a reason for most, if not all stellar variability (with the main exception being eclipses being used to describe Algol-like light curves), came to an abrupt end with the advancements of spectrometry and photometry occurring in the late 19th and early 20th centuries. Discoveries in stellar characteristics, including but not limited to, pulsations, eclipsing binaries, supernovae, and rotational properties, led to the so-called “downfall” of starspots being the main explicative factor to the significant periodic magnitude changes astronomers were observing at the time. It was not until the mid-20th century that starspots were once again used to denote stellar variability not explicitly explained by pulsations or the nature of eclipsing binaries. In 1945, American astronomer Gerald E. Kron was the first to correctly attribute stellar variations to starspots that were decidedly causing said variations on the binary systems of RS Andromadae, RS Canum Venaticorum, YY Geminorum, and AR Lacertae. Later conclusions concerning the presence of starspots and their effect on solar magnitude variability were derived from noteworthy photoelectric light curves of RS Canum Venaticorum spanning from 1963 to 1968. These light curves explicitly detailed the magnitude variance of RS Canum Venaticorum as a result of starspots occurring on its surface, a conclusion Kron had outlined roughly twenty years earlier. The culmination of conclusions made from these observations and ones occurring earlier re-sparked the astronomical interest in starspots as a major component of overall stellar variability, with modern starspot detection expanding through the development of several detection methodologies (Hall, 1994, Ret. April 29, 2024).

1.4 Starspot Detection

Unlike sunspots, which can be easily detected and imaged directly using present-day telescopes and satellites, starspots are difficult to image directly in the optical (Giles et al., 2017, Ret. April 29, 2024). Their distance and relative size on the surface of stars currently of interest prevent traditional optical methods of sunspot detection and imaging from successfully discerning starspots from other solar-like activities (Center for Astrophysics | Harvard & Smithsonian, 2017, Ret. April 29, 2024). Despite these challenges, starspots have been detected on stars of varying types using a multitude of detection methodologies. Detection and characterization of starspots is dependent on the nature of the star being observed. A description and analysis of the most common approaches to starspot detection are found below.

Doppler Imaging (DI)

Doppler Imaging (DI) is "currently the highest resolution indirect imaging technique in astrophysics," and is used to detect variations in temperature, brightness, magnetic field activity, and other stellar variations (Kochukhov, n.d., Ret. April 29, 2024). The first starspots to be detected using Doppler Imaging were documented by University of California astronomers Steven S. Vogt and G. Donald Pernod in 1983 (Vogt & Penrod, 1983, Ret. April 29, 2024). As adopted in the Vogt and Pernod observation, DI makes use of the well-documented Doppler effect, a direct consequence of stellar rotation (Kochukhov, n.d., Ret. April 29, 2024). Each star is known to have its own unique spectral appearance that can be observed from Earth. A given star's spectrum is dependent upon several factors including (but not limited to) the star's density, temperature, chemical composition, and motion (AURA Space Telescope Science Institute, 2022, Ret. April 29, 2024). Star rotation induces the Doppler Effect, with the portion of the star rotating away from an observer causing a "redshift" in the observed spectrum of the star, and the portion towards an observer causing a "blueshift" in the observed spectrum. One can one-dimensionally map the overall changes of a star's spectrum as a given wavelength is emitted across the star's surface, thus creating a spectral line. Any substantial change in wavelength due to an obscuration or temperature change causes a graphical dip or rise in the associated spectral line. Starspots' significantly lower surface temperature and brightness result in a distortion of the disk-integrated stellar spectral line profile of a star being observed (Kochukhov, n.d., Ret. April 29, 2024). This distortion, or starspot, tracks across the spectral line as the star rotates. A starspot's time-specific longitude on its parent star's surface can be resolved by its coordinate location along the star's distinct spectral line. Though not as precise as its longitude, a starspot's latitude can be implied from the spot's amplitude and speed across its parent star's spectral line. The degree to which a spot appears as a distortion on its parent star's spectral line is dependent upon the angle at which the axis of rotation of the star is viewed from the Earth, as well as the

star's rotational period. Stars with stellar inclinations (i) of $i = 0°$ make DI impossible due to a lack of Doppler broadening. Stars with $i = 90°$ make distinguishing a spot located on the northern (upper) hemisphere versus a spot located on the southern (lower) hemisphere unattainable. Stellar inclinations ranging from $30° \leq i \leq 90°$ are most desirable for DI. With one hemisphere always being slightly obscured, distortions resulting from starspots become easier to identify and locate on the surface of the star being observed. Stars acceptable for DI must also have considerably fast rotational velocities. Faster rotational velocities increase spatial resolution, making resulting images easier to resolve. Faster rotational velocities do, however, produce smaller spectral line depths that consequently require higher signal to noise ratios (S/N) to accurately resolve spot distortions. To effectively balance starspot resolution with noise, it is desirable to observe stars that have rotational velocities ranging from 40 - 80 km/s when using DI (Vogt & Penrod, 1983, Ret. April 29, 2024). In the case of a star whose axis of rotation is tilted towards an observer on Earth, a spot of higher latitude tends to result in a distortion found on the star's spectral line that is visible for more than half of the star's rotational period. A spot of lower latitude tends to result in a distortion found on the star's spectral line that is visible for a time equal to one-half of the star's rotational period and would be observed as moving from the blue-shifted region of the star to the red-shifted region. These spectral line properties are reversed for stars whose axis of rotation is angled away from an observer on Earth. Multiple observations at varying times can be used to determine a starspot's relative position on its parent star to a reasonable degree of accuracy (Rice, 2014, Ret. April 29, 2024). Plotting a distortion, or starspot onto a star's surface through the above process creates what is known as a Doppler Image (DI) of a starspot. Below is an illustration of a hypothetical starspot that is observed to move across its parent star's spectral line profile in the form of a distortion in wavelength. The spot is pictured moving from the blue-shifted region of the star to the red-shifted region of the star due to the Doppler effect. Above the star's spectral line is the resulting DI (Kochukhov, n.d., Ret. April 29, 2024).

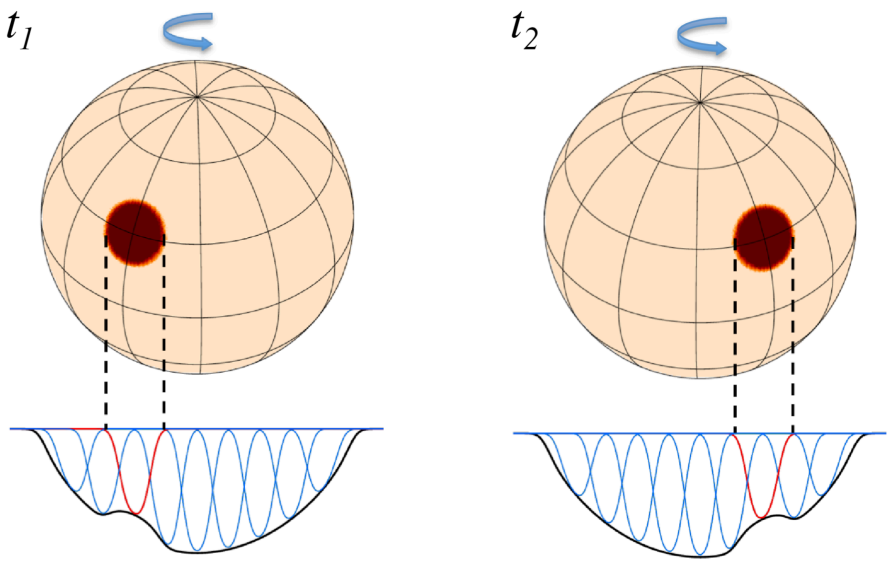

Figure 7: Spectral line of star, with distortion in wavelength appearing as a starspot moves across the star's surface over the course of a rotational period (Kochukhov, n.d., Ret. April 29, 2024).

As noted above, "standard" Doppler Imaging is limited to analyzing only rapidly rotating stars. An extension of DI, known as Zeeman Doppler Imaging (ZDI), is not limited to rapidly rotating stars due to its adherence to both Doppler resolution and rotational modulation of polarimetric signatures. Though more instrument and power-intensive, ZDI has been successfully used to detect sunspots and other solar variations as a result of the solar magnetic dynamo (Kochukhov, n.d., Ret. April 29, 2024). It has also been cited as an effective detection methodology for sunspot characteristics, including temperature and polarity parameters (Hackman et al., 2016, Ret. April 29, 2024).

Eclipse Mapping

Detection of starspots through eclipse mapping involves light curve analysis of magnetically-active binary star systems. Magnetically active stars are often detected in close-binary systems. Stars in these systems often present high rotational rates due to considerable tidal interactions taking place between the pair(s). Binaries that satisfy these characteristics and orbit one another with edge-on inclination will present eclipses observable through light curve analysis. Starspots present on the eclipsed hemisphere of either star in the binary system will appear as distortions on the observed star's spectral eclipse line. Like Doppler Imaging, the information gathered from light curve analysis of eclipsing stars can be used to create a tomographic map of the detected starspots. The figure below depicts an eclipse mapping of two main sequence stars in the XY Ursae Majoris system. Starspots are seen clearly as dark regions on the hotter primary star as the smaller, cooler child star eclipses (Cameron, 2000, Ret. April 29, 2024).

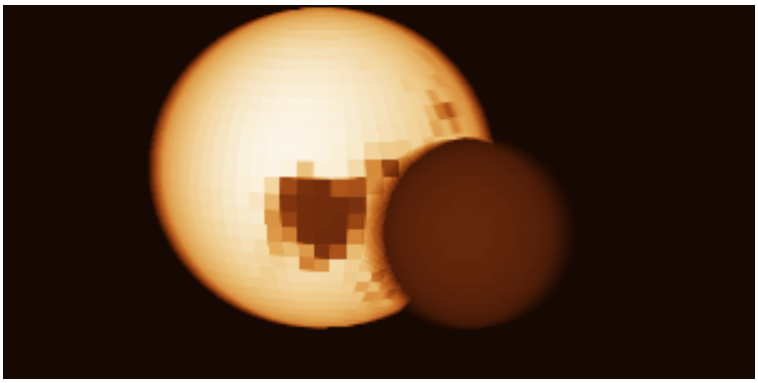

Figure 8: Eclipse mapping of XY Ursae Majoris system using V-band light-curve analysis, with starspots present on the larger parent star (Cameron, 2000, Ret. April 29, 2024).

Eclipse mapping has a distinct advantage over Doppler Imaging in detecting starspots on or near the equator of a given star being observed. As detailed above, DI cannot differentiate between starspots occurring in northern (upper) hemispheres versus southern (lower) hemispheres of stars with stellar inclinations equal to 90° (Vogt & Penrod, 1983, Ret. April 29, 2024). Eclipse mapping's reliance on eclipse inclination comparatively allows observers to detect and accurately locate starspots occurring on the equatorial line of a given star. Binary systems that eclipse edge-on exhibit transiting belts near or around the parent star's equator. From there, spectral analysis and eclipse mapping can be used to accurately discern starspots' latitudinal coordinates near the star's equator - a feat that is impossible for DI.

Eclipse mapping also reveals promising opportunities for further study of the variability of stars similar in type to the Sun. Accurate sunspot number, location, and area calculations, specifically maintained by the Royal Greenwich Observatory since 1874, have revealed distinct characteristics of sunspots that are dependent upon the Sun's solar variability cycle stage. Precise sunspot positional data has shown two specific latitude bands that sunspots are most likely to occur during a given solar cycle. When graphed with latitude as a function of time, little to no sunspots are found at latitudes ≥ 40°, with most sunspots specifically occurring near or on the equator (latitude = 0°) during solar maxima (Charbonneau & Wright, 1995, Ret. April 29, 2024). This graph, known as the "Butterfly Diagram," is pictured below, with an additional diagram depicting average daily sunspot area as a function of time (Hathaway, 2017, Ret. April 29, 2024).

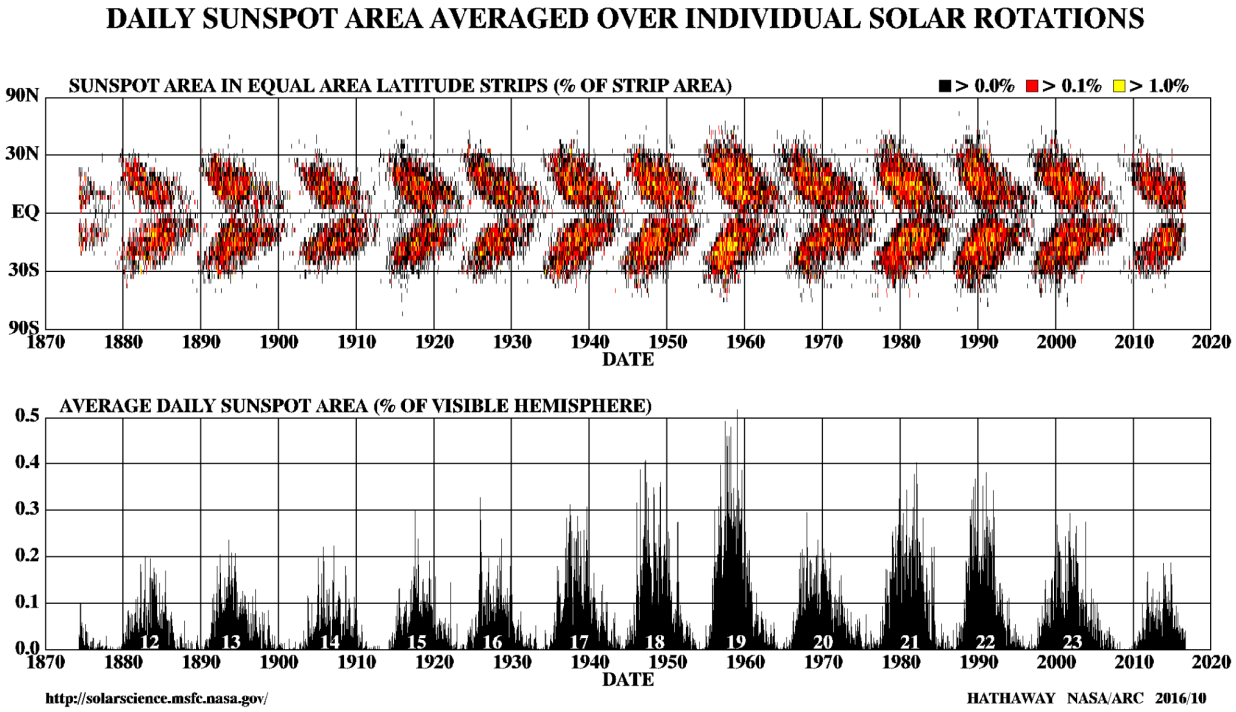

Figure 9: Top; "Butterfly Diagram," a graphical representation of sunspot area in equal area latitude strips as a function of time. Bottom; Graphical representation of average daily sunspot area (% of visible hemisphere) as a function of time (Hathaway, 2017, Ret. April 29, 2024).

Extended observations of solar-like eclipsing binary systems could reveal sunspot nature similar to that presented above in the "Butterfly Diagram." While conclusions of the nature of overall stellar variability of stars similar in type to the Sun would require extensive observation, eclipse mapping presents itself as a valuable starspot detection method, and could potentially serve as an instrumental observational technique in understanding main sequence starspot variability. Further analysis of this detection and interpretational method, as well as its relevance to other forms of

stellar variability, is found below in the Comparison Analysis section of this thesis (Wolter et al., 2009, Ret. April 29, 2024).

Line Depth Ratio (LDR)

Line depth ratio analysis is often employed to detect starspots on larger stars with slower rotational velocities and longer rotational periods. Stars with slower rotational velocities result in less spatial resolution, making detection methodologies such as Doppler Imaging and Eclipse Mapping nearly obsolete for these types of stars (Vogt & Penrod, 1983, Ret. April 29, 2024). Line depth ratio analysis does not suffer from the above resolution issue, and instead involves the comparison of two absorption bands of magnetically-active stars (O'Neal, 2006, Ret. April 29, 2024). As with sunspots, starspots are known to be significantly cooler in temperature compared to the surface temperatures surrounding a given starspot (Center for Astrophysics | Harvard & Smithsonian, 2017, Ret. April 29, 2024). LDR analysis takes advantage of this principle by comparing a given star's two atomic absorption bands, with one of these bands being sensitive to temperature, and the other band not being responsive to temperature. Spectroscopic analysis through LDR of these two bands can then be used to detect the temperature difference between the surface of the star and a potential starspot. LDR analysis suffers from considerable accuracy concerns regarding the temperature of a detected starspot. Stars with spots closely grouped can be difficult to distinguish individually due to blending and resolution challenges. LDR-observed stars with faster rotational velocities commonly experience this blending problem, with starspot temperatures often measuring much different than their expected error-inclusive values in comparison to spots found on slower-rotating stars. Starspots with temperatures less than 4000 K are generally undetectable through LDR analysis. This is because atomic lines used in LDR analysis often blend strongly with titanium oxide (TiO) absorption spectra, an absorption band used regularly in starspot detection via LDR. Starspots with atomic lines near and around 6140 Å merge with TiO resulting in the spots becoming imperceivable within the total spectrum of the star being observed (O'Neal, 2006, Ret. April 29, 2024). The overall efficacy of line depth ratio analysis in terms of starspot detection is examined further in the below "Comparison Analysis" section. Its detection performance of other forms of stellar variability is also addressed in this section.

Interferometry

Starspot properties including number, area, temperature, and location can be reasonably inferred through long-baseline optical and near-infrared interferometry (LBI) (Parks et al., 2021, Ret. April 29, 2024). Concerning starspot detection, interferometry differs from the above methodologies, as it is a form of direct observation through optical and near-infrared analysis. LBI requires an array of several distantly positioned optical and infrared telescopes and specifically makes use of the wave nature of light, originally discovered and detailed by Thomas Young in 1803 (Monnier, 2003, Ret. April 29, 2024). Incoming light from a point source (star) is "delayed" such that light entering one telescope of a given array has an equal path compared to its "paired" telescope. Once all telescopes within the array demonstrate equal light paths, light entering each telescope is combined to create a resulting interference fringe. Further analysis of this fringe and measurement of observed interference patterns allows for the reconstruction of the given star's surface in a two-dimensional form factor. Through image reconstruction, one can examine the observed star's surface temperature and brightness variations and make accurate inferences about the existence, size, location, and period of starspots present on the said star's surface. The figure below is the result of a 2021 publishing titled, "Interferometric Imaging of λ Andromedae: Evidence of Starspots and Rotation." The image depicts several stellar surface images of the star λ Andromedae reconstructed through past interferometric observations. Starspots are depicted on the surface of λ Andromedae (Parks et al., 2021, Ret. April 29, 2024).

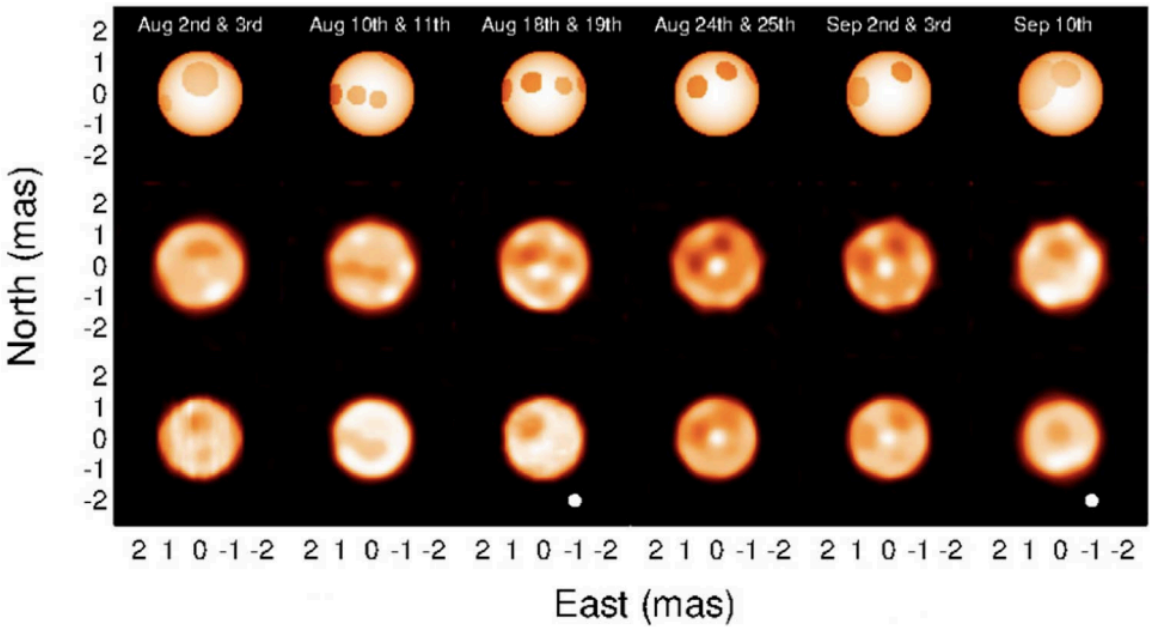

Figure 10: “Stellar surface images for the 2010 data set. The top row contains the model images, the middle row contains the reconstructed images, and the bottom row contains the simulated images” (Parks et al., 2021, Ret. April 29, 2024).

Interferometry is perhaps the most promising methodology for future starspot detection. Interferometric data can easily be compared to photometric observational measurements to conclude the validity of rotational period predictions and starspot motion. Additionally, due to LBI’s autonomy from absorption-line analysis, starspot detection through this approach is not limited to faster-rotating stars (While Doppler Imaging is velocity-limited due to the widening of absorption lines at slower rotational velocities). Though currently limited to ground-based optical and near-infrared arrays, interferometry has proven successful in identifying starspot characteristics of stars exhibiting stellar variability (Parks et al., 2021, Ret. April 29, 2024). In the context of both starspots and other forms of stellar variability, this detection technique is scrutinized in further detail in the following Comparison Analysis section.

Comparison Analysis

Historically, the detection methodologies outlined above have revealed a multitude of information about starspots. While specific characterizations of starspots depend upon the detection technique applied, details on starspot size, location, temperature, and evolution have been documented, especially over the last twenty years. Other manifestations of stellar variability have been detected and outlined as a result of the growing interest in starspot academia. The following is a comparison analysis of a collection of recent publications on starspot observations. This includes a summary of astronomical findings, synopses of detection methodologies, and potential implications of these observations in relation to overall stellar variability and the Sun’s evolutionary dynamics.

2.1 Transit Mapping Analysis

Presented below are the findings of U. Wolter et al., a 2009 publication on, “Transit mapping of a starspot on CoRoT-2: Probing a stellar surface with planetary transits” (Wolter et al., 2009, Ret. April 29, 2024). CoRoT-2 is a G7V class, a yellow dwarf main sequence star about 700 ly away from the Earth (Strasbourg astronomical Data Center, n.d., Ret. April 29, 2024). Its similarity in type to the Sun makes it not only ideal for stellar variability analysis, but also exoplanet detection. “Transit lightcurves of CoRoT-2b, a massive hot Jupiter orbiting [CoRoT-2],” were specifically analyzed in this publication. The CoRoT space satellite responsible for the light curve observational data of this publication explicitly observed from 2007 May 16 to 2007 October 15, encompassing 31 stellar rotations of CoRoT-2 and 79 total planetary transits of CoRoT-2b.

After normalization of the observational light curve data, a narrow-featured spot-like feature was detected during a particular transit of CoRoT-2b. Normalized light curve data of this transit, documented as “transit 56,” revealed the “most pronounced and isolated “bump” of the whole time series of CoRoT-2, suggesting a relatively narrow spot occulted close to the disk center.” The graphical representation of this light curve data is presented below.

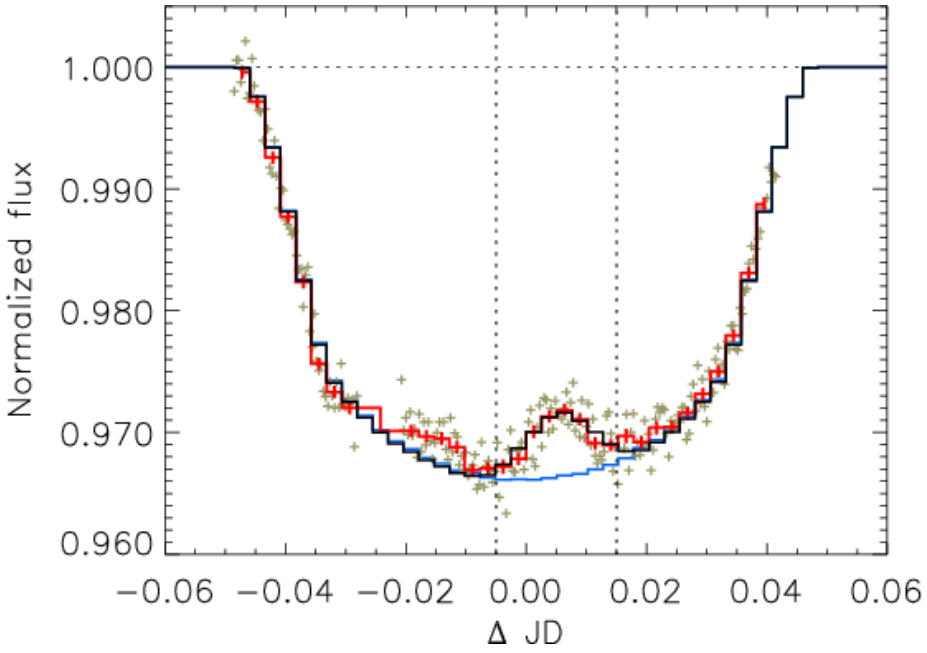

Figure 11: “Normalized lightcurve during ‘transit 56’, as a function of time from the transit center. The blue line shows the transit model for an unspotted star for comparison. The shallow deformation left of the transit center is caused by another spot not included in [this] model” (Wolter et al., 2009, Ret. April 29, 2024).

From this light curve analysis, several informative parameters of this star spot were able to be inferred, including spot radius r, central longitude ϕ, and colatitude θ. The well-defined nature of the transit distortion (starspot) belonging to “transit 56” resulted in the spot’s longitude being narrowly bound to the transit light curve. Spot radius r and colatitude θ were calculated for both “dark spot” and “bright spot” scenarios. The “dark spot” scenario assumed a spot flux of 30% of the photospheric flux of CoRoT-2, with the “bright spot” scenario assuming a spot flux of 75% of the photospheric flux of CoRoT-2. This association is roughly comparable to the spot flux of sunspots of varying areas and strengths (Wolter et al., 2009, Ret. April 29, 2024; Walton et al., 2003, Ret. April 29, 2024; Albregtsen et al., 1984, Ret. April 29, 2024). Further rebinning of “transit 56’s” light curve, along with error estimation via Gaussian error propagation, revealed the following parameters of the spot via transit mapping analysis.

Model[a]	Long.	Colat.	Radius	Flux[b]	χ^2	Area[c]
BC	216.4°	75.0°	7.8°	0.75	0.8	0.45%
BN	216.5°	70.0°	9.5°	0.75	1.4	0.55%
BS	216.2°	80.0°	8.5°	0.75	1.2	0.47%
DN	216.7°	71.0°	4.8°	0.3	1.7	0.18%
DS	216.2°	81.0°	4.8°	0.3	1.9	0.18%
DEQ	216.3°	94.0°	15.3°	0.3	1.6	0.72%

Figure 12: "Parameters of characteristic spot solutions discussed in the text; longitudes and colatitudes are given for the spot center" (Wolter et al., 2009, Ret. April 29, 2024). Note: "BC, BN, and BS stand for "bright central", "bright north" and "bright south", respectively. They describe spots with colatitudes close to the center of the planetary disk. DN and DS stand for "north" and "south" dark spot solutions, respectively; DEQ represents a "dark" spot centered below the equator. *b* Relative to the photosphere. $\mathcal{D}^2$ goodness of fit between *r* and θ. *c* Fraction of total stellar surface" (Wolter et al., 2009, Ret. April 29, 2024).

It is clear from this publication alone that much can be inferred about a star spot's characteristics through transit mapping analysis. While this detection methodology requires many of the same stellar and eclipsing body inclination conditions noted for "Doppler Imaging," it can be applied easily to past spectral analyses of systems that meet said observational criteria. The most intriguing notion about this transit mapping analysis is the confirmation of stellar variability of a star similar in type to the Sun. Continued observation and evaluation of G-type stars via transit mapping analysis could very likely lead to a more comprehensive understanding of the nature of starspots and other instances of stellar variability. This success does, however, introduce the natural overlap between starspot and exoplanet observation, both of which rely heavily on this detection methodology (Vogt & Penrod, 1983, Ret. April 29, 2024). While transit mapping analysis will likely play a major role in future detections and publications concerning starspots, one must acknowledge transit mapping analysis' inherent introduction of error, biases, and misconceptions as a result of this overlap. Complications from this intersection of interests are described in greater detail in the following "Exoplanets: A Challenge of Shared Interests" section.

2.2 Line Depth Ratio Analysis

Detection and analysis of starspots through Line Depth Ratio (LDR) has been shown to be severely problematic. Whereas transit mapping analysis has shown promising results detecting starspots on highly active stars with short rotational periods, LDR "encounters serious difficulties when used for heavily spotted active stars" (Vogt & Penrod, 1983, Ret. April 29, 2024). These challenges are exemplified by the findings of author Douglass O'Neal in his LDR Analysis publication titled, "On the Use of Line Depth Ratios to Measure Starspot Properties on Magnetically Active Stars" (O'Neal, 2006, Ret. April 29, 2024). The following is a summary of

the findings of O'Neal regarding the concerns LDR presents when used as a starspot detection methodology.

Average surface temperatures of numerous active stars were documented previously via LDR by Catalano et al. (Catalano et al., 2002, Ret. April 29, 2024). O'Neal sought to reproduce the results of Catalano et al. through a comparison LDR analysis of several active and inactive comparison stars. Spectra of these stars were obtained in TiO bands at 7055 and 8860 Å, with spectra also gathered near 6200 Å (McCarthy et al., 1993, Ret. April 29, 2024). Atomic lines adopted by Catalano et al. were included in O'Neal's analysis. Below is Figure 13, a table of the properties of the active stars used in O'Neal's publication in terms of spectral findings in the stated TiO and resulting LDR determinations. Figure 14 depicts the properties of the comparison stars analyzed by O'Neal in the 6200 Å region.

TABLE 1
PROPERTIES OF ACTIVE STARS

Name	Spectral Type	Date of Observation (2002 Dec)	$v \sin i$ (km s^{-1})	P_{rot} (days)	T_Q (K)	T_S from TiO (K)	f_S from TiO	T_m from LDR (K)
II Peg	K2 IV	21, 22, 25, 26	23	6.72	4800[a]	3425 ± 75	0.43–0.54	4482–4583 ± 100[b]
λ And	G8 III	21	6.5	53.95	4700[c]	3600 ± 50	0.32 ± 0.06	4672 ± 43
DM UMa	K2 III–IV	21	26	7.49	4500[d]	3300 ± 100	0.37 ± 0.05	4655 ± 75[e]
								4743 ± 53[f]
IM Peg	K1.5 III	25	26	24.65	4450[g]	3400 ± 125	0.20 ± 0.05	4594 ± 94
LQ Hya	K0 V	25	25	1.6	5180[h]	3400 ± 150	0.49 ± 0.06	5112 ± 113
VY Ari	K3–4 V–IV	22	6.9	16.2	4916[i]	3250 ± 125	0.51 ± 0.05	5071 ± 83[j]
						3650 ± 100	0.32 ± 0.04	4779 ± 99[e]

Figure 13: "Properties of Active Stars."

[a O'Neal et al. (1996). b Range of values in last two columns represents different nights of observation. c O'Neal et al. (1998). d O'Neal et al. (2004). e Fits using giant comparison stars. f Fits using subgiant comparison stars. g Berdyugina et al. (1999b). h Saar et al. (2001). i C02. j Fits using dwarf comparison stars. Note: superscripts found for values in columns labeled T_Q and T_m from LDR (O'Neal, 2006, Ret. April 29, 2024).]

TABLE 2
PROPERTIES OF COMPARISON STARS OBSERVED IN 6200 Å REGION

Name	HR	Spectral Type	$T_{\rm eff}$ (K)	Distance (pc)	V	M_V	ΔM_V
			A. Dwarfs				
Sun	...	G2 V	5800	...	−26.8	4.83	−0.2
σ^2 Eri	1325	K1 V	5175	4.95	4.43	5.96	−0.3
(none)	2692	G9 V	5100	41.7	6.43	3.33[a]	...
γ Lep B	1982	K2 V	4950	8.20	6.15	6.58	−0.1
(none)	1614	K3 V	4750	9.43	6.23	6.36	−1.0
Gl 570A	5568	K4 V	4575	5.68	5.72	6.95	−0.85
Gl 338A	...	K7 V	3800	6.21	7.64	8.67	−1.4
Gl 488	...	M0 V	3700	11.5	8.49	8.19	...
Gl 400A	...	M2 V	3600	...	9.30	10.0[b]	...
			B. Subgiants				
(none)	3762	G6 IV	5100	54.4	6.25	2.57	−3.8
(none)	2660	G8 IV	4975	30.3	5.55	3.14	−3.5
o Col	1743	K0 IV	4800	33.7	4.82	2.18	−5.1
γ Cep	8974	K1 IV	4775	15.6	3.21	2.24	−5.1
(none)	5227	K2 IV	4475	43.5	6.34	3.15	−4.8
			C. Giants				
10 LMi	3800	G8 III	5025	54.0	4.58	0.92	−5.6
δ Aur	2077	K0 III	4850	50.0	3.74	0.25	−6.8
δ Ari	951	K2 III	4800	40.0	4.35	1.34	−6.0
χ Gem	3149	K2 III	4600	71.4	4.96	0.69	−7.0
σ Hya	3418	K1 III	4450	40.0	4.45	1.45	−6.5
κ Leo	3731	K2 III	4375	65.4	4.47	0.39	−6.5
ν UMa	4377	K3 III	4125	71.4	3.51	−0.76	−7.6

Figure 14: “Properties of Comparison Stars observed in 6200 Å Region.”
[a HR 2692 has possibly been misclassified in the literature and might be a subgiant instead (based on M_V). This does not substantially affect our analysis. b Estimated from spectral type (O'Neal, 2006, Ret. April 29, 2024).]

Examination of these properties revealed three major complications of LDR analysis. Firstly, values calculated via LDR were found to be heavily dependent on the rotational velocity of the star being observed. The spectral line occurring at λ6243, originally outlined by Catalano et al., was found to suffer from severe blending issues, with blending being especially evident amongst the spectra of the observed active stars (Catalano et al., 2002, Ret. April 29, 2024). LDR analysis of these spectrally blended stars resulted in calculations of T_m being 100–150 K higher than reality. Heavy blending of the TiO bands was also observed for active stars. “Contamination of the atomic lines by TiO in the star’s spotted regions” likely resulted in LDR measurements of T_S being, “300–500 K greater than values measured from TiO bands.” This is especially concerning for starspot detection, as TiO bands are commonly observed in cooler stellar regions, such as starspots. Finally, values computed via LDR were found to be incapable of reproducing test (simulated) spectra inputs. LDR consistently overestimated T_S values of artificial test star spectra in comparison to real spot proxy values that garnered values more consistent with simulated input values (O'Neal, 2006, Ret. April 29, 2024).

Line Depth Ratio analysis undoubtedly suffers from major quantitative shortfalls regarding the detection and characterization of active stars. The extent of these inaccuracies is evidently dependent upon a given star's rotational velocity, a quantity consistently faster in active stars that exhibit more frequent occurrences of starspots. As noted by O'Neal, starspot and general stellar figures determined by LDR analysis must be scrutinized, especially when the stars being observed are of active type (O'Neal, 2006, Ret. April 29, 2024). Future starspot investigations on stars similar in type to the Sun should consequently be completed using methodologies other than Line Depth Ratio analysis so as not to introduce imprecision into starspot analytics.

2.3 Interferometry Analysis

Interferometry has exhibited recent promise as a successful starspot detection and analysis methodology (Roettenbacher et al., 2016, Ret. April 29, 2024; Roettenbacher et al., 2017, Ret. April 29, 2024). This thesis outlines the 2021 findings of authors J. R. Parks et al. in their publication, "Interferometric Imaging of λ Andromedae: Evidence of Starspots and Rotation." J.R. Parks et al. analyze λ Andromedae, a single spectroscopic binary with considerable activity on the larger parent star of the system (Walker, 1944, Ret. April 29, 2024). Interferometric data of λ Andromedae was gathered over 26 nights from 2008 August 17 to 2011 September 24, with observations taking place using the "Center for High Angular Resolution Astronomy (CHARA) array owned and operated by Georgia State University" (Parks et al., 2021, Ret. April 29, 2024).

The characterization of starspots found on the larger parent star of the λ Andromedae system was completed using two independent approaches including the "spotted star model" and "image reconstruction." The "spotted star model" created a simplified surface model of λ Andromedae using limb-darkening data collected via CHARA. The model specifically discerns potential areas of greater starspot concentration to estimate, "covering factor (ϕ), starspot latitude (b), starspot longitude (l), and the starspot intensity ratio (f)." Further reduction and analysis of the combined 2010 and 2011 interferometric data revealed these parameters for individual starspots occurring, with models "limited only to one, two, or three starspots" achieving the greatest degrees of success without introducing irreversible levels of error. Image reconstructions of the observed starspots were created independently of the above "star spotted model" method. Instead, flux elements contained in the observed interferometric data are "regularized" using the code "SQUEEZE" cited by Baron et al in a similar 2010 publication (Monnier et al., 2006, Ret. April 29, 2024). As noted in the J. R. Parks et al. publication, "A final image reconstruction is the average of 10 images generated by SQUEEZE" (Parks et al., 2021, Ret. April 29, 2024).

To not introduce bias from the data-sampling and image reconstruction process of the observed starspots, a third and final simulated image reconstruction process was adopted. "Bright spot features" such as stellar flares and plage, were of concern amongst the reconstructed images due

to the challenge of discerning observed flares and plage from “bright spots” created as a consequence of the image reconstruction process. Stellar surface images of λ Andromedae from both the 2010 and 2011 datasets are depicted below. These images include the modeled surfaces, reconstructed surfaces, and simulated surfaces of λ Andromedae over the two datasets. [Note: “Artifacts due to miscalibrated observables will be features seen in the reconstructed image, but they are absent in both the simulated and model images” (Parks et al., 2021, Ret. April 29, 2024).]

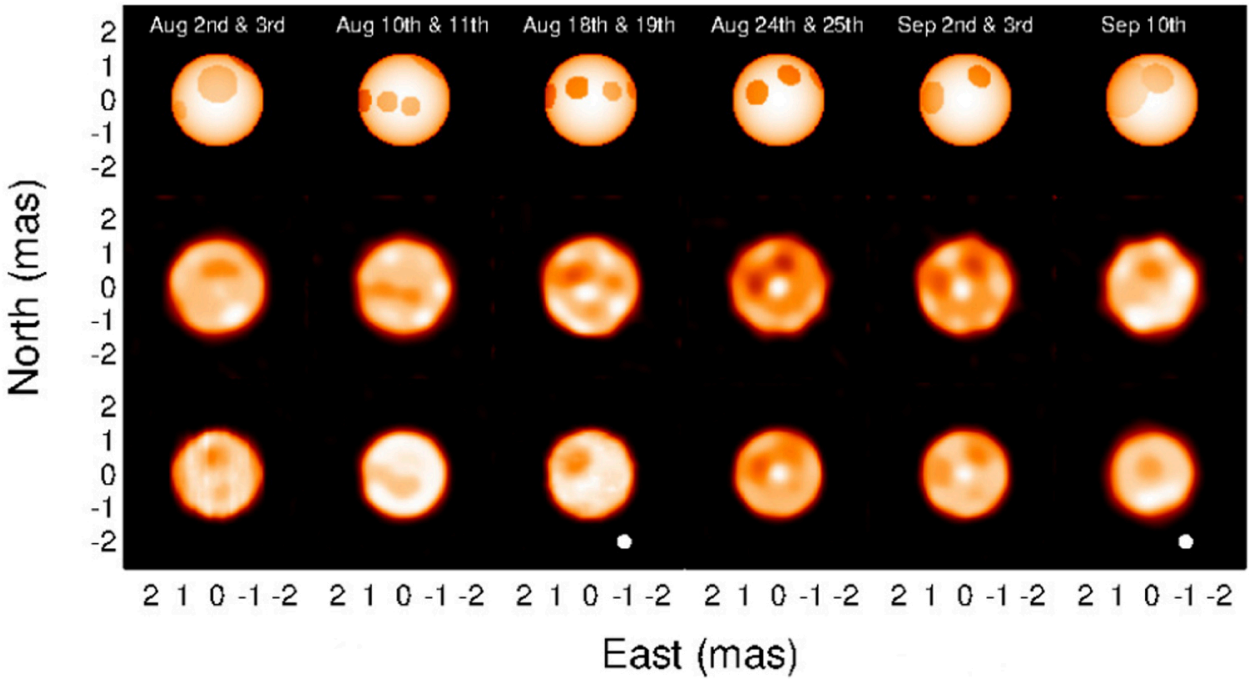

Figure 15: “Stellar surface images for the 2010 data set. The top row contains the model images, the middle row contains the reconstructed images, and the bottom row
contains the simulated images. The white dot in the lower right corner represents the 0.4 mas resolution limit for the CHARA array” (Parks et al., 2021, Ret. April 29, 2024).

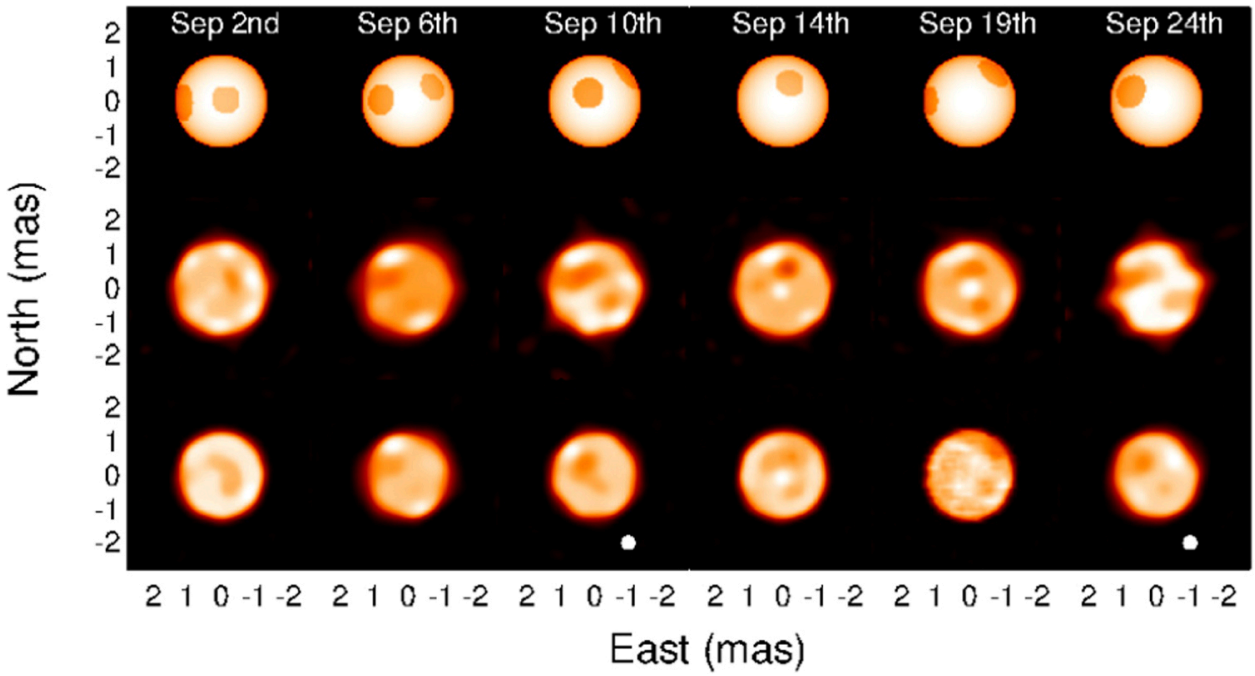

Figure 16: "Stellar surface images for the 2011 data set. The top row contains the model images, the middle row contains the reconstructed images, and the bottom row contains the simulated images. The white dot in the lower right corner represents the 0.4 mas resolution limit for the CHARA array" (Parks et al., 2021, Ret. April 29, 2024).

The images above serve as encouraging representations of starspot detections through interferometry analysis. Modeled flux variability of λ Andromedae was found to be consistent with photometric time series measurements gathered previously. Uniformities in spot features, occurrences, and flux variability between the two datasets were also documented. Calculation of λ Andromedae's rotational period via observed starspot rotational characteristics also proved successful, with the "2011 period [being] nearly identical to the photometric period." While this publication cites its preliminary nature, the agreement between interferometric conclusions and previous photometric documentation of λ Andromedae is reassuring. Results from this publication and others favor future interferometry analysis of starspots as a direct-imaging detection methodology capable of characterizing starspots and calculating stellar parameters of active stars (Parks et al., 2021, Ret. April 29, 2024). A more comprehensive understanding of starspots and overall stellar variability of stars similar in type to the Sun is likely to develop if results from future interferometry analysis publications are consistent with those gathered via Doppler Imaging and photometry.

Exoplanets: A Challenge of Shared Interests

The nature of starspots presents a difficult overlap with other solar variability phenomena, but also poses a great deal of misleading observational overlap with exoplanets. Starspot detection via light curve analysis exemplifies this challenge, with starspots and other instances of stellar variability oftentimes hampering the degree to which exoplanet existence can be confirmed (Medina et al., 2020, Ret. April 29, 2024).

3.1 Occluding Starspots

The detection of exoplanets outside of the Solar System is commonly documented through transit light curve analysis, as is the detection of starspots. Groundbreaking photometric surveys via the likes of Kepler, the Transiting Exoplanet Survey (TESS), and now through the James Webb Space Telescope (JWST) have resulted in the confirmation of over 5,000 exoplanets (Bolles, 2024, Ret. April 29, 2024). While transit light curve analysis can provide crucial astrometric data about exoplanet sizes, orbital period lengths, and average distances to a given parent star, sources of occlusion or spikes in incoming flux can hamper its ability to make astrometric inferences (NASA Ames, 2024, Ret. April 29, 2024). This impact is known as the "Transit Light Source Effect," and is especially influential in the observation of exoplanets orbiting M-type stars due to their heightened stellar variability (Apai et al., 2018, Ret. April 29, 2024). Stellar contamination from both small and large starspot groups has been documented to cause inaccuracies in exoplanet radius estimations and consequential density miscalculations. Solar-like spot cases have been shown to "mask" common spectral exoplanet features, thus leading to smaller radii calculations and larger density assumptions. Transit depth change due to starspots is sometimes so drastic that planetary atmospheric characteristics are mistaken for other transmission properties, or are simply masked entirely. Low-mass exoplanetary systems of interest, such as the regularly cited TRAPPIST system, will likely require re-examination of their physical characteristics originally obtained through Kepler and TESS light curve analysis. Future photometric JWST inferences made based upon past Kepler and TESS observations should be evaluated with some skepticism so as to not introduce a stellar variation dependency bias in radius and density calculations of observed exoplanets (Rackham et al., 2018, Ret. April 29, 2024).

3.2 Other Stellar Variability Examples

In addition to starspot detection, Kepler and TESS light curve analysis has proven as an effective detection methodology for other forms of stellar variability. Instances of stellar flaring have been documented through the examination of outlier brightness increases in M-type star light curves. Light curve analysis has been used to outline the relationship between stellar type and flare frequency and strength. Older stars with longer rotational periods (similar to the Sun) have been

shown to flare less frequently due to a lack of magnetic dynamo variability, a consequence of the loss of angular momentum as a given star ages. M-type stars, however, have been documented to flare with frequencies higher than the Sun due to their higher rotational velocities. This finding is significant in terms of exoplanet detection and research, as flare strength and frequency may play a role in the habitability of a given exoplanet during the lifetime of its parent star (Davenport, 2016, Ret. April 29, 2024). Excess Hα line emission and near-infrared wavelength emission common in flare and superflare instances have been shown to contaminate absorption wavelengths of CO2. These absorption wavelengths are imperative features for exoplanet light curve analysis, especially regarding the potential habitability of exoplanet systems such as TRAPPIST (Howard et al., 2023, Ret. April 29, 2024; Araújo & Valio, 2021, Ret. April 29, 2024). Continued analysis of past Kepler and TESS light curve data, as well as newly collected photometric data from JWST, will likely be required to achieve a more conclusive understanding of the degree to which stellar variability affects exoplanet detection, as well as how features such as starspots and flares may impact the habitability of detected exoplanets in terms of our current knowledge of the requirements for life (Medina et al., 2020, Ret. April 29, 2024).

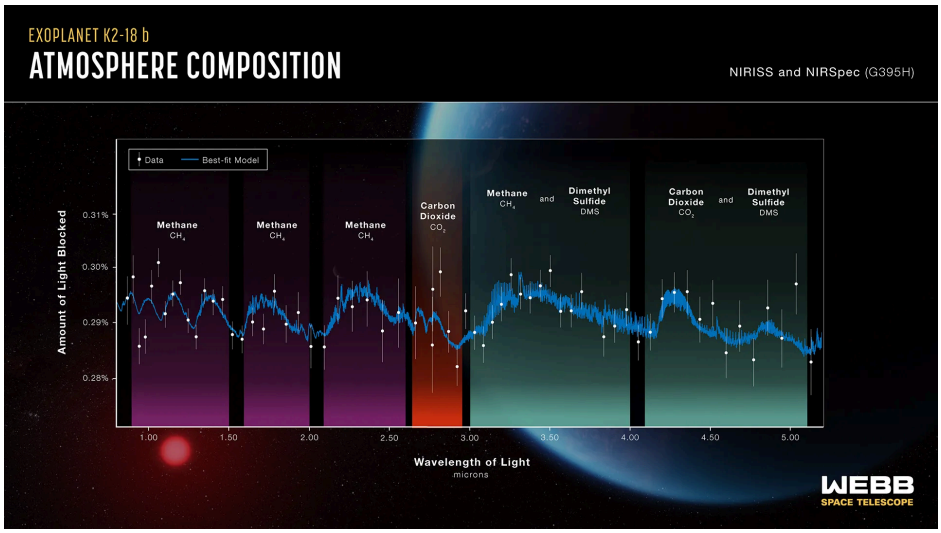

Figure 17: “Spectra of K2-18 b, obtained with Webb’s NIRISS (Near-Infrared Imager and Slitless Spectrograph) and NIRSpec (Near-Infrared Spectrograph)” (Bowman & Sabia, 2023, Ret. April 29, 2024). Excess Hα line emission and near-infrared wavelength emission common in flare and superflare instances have been shown to contaminate absorption wavelengths of CO2. Re-analysis of spectral lines similar to the figure above may be required as a result of contamination (Howard et al., 2023, Ret. April 29, 2024; Bowman & Sabia, 2023, Ret. April 29, 2024).

Conclusions

- Recent innovations in spectral analysis have proven successful in detecting starspots present on the surfaces of stars similar in type to the Sun.
- Success in starspot detection has not been limited to a singular detection methodology. Instead, several detection methods with varying approaches and procedures have been deployed with conclusive results of starspots occurring on stars other than the Sun.
- Detection methodologies, including, but not limited to, Doppler Imaging, Eclipse Mapping, Line Depth Ratio analysis, and Transit Mapping, have each had differing degrees of historical success regarding the detection of starspots. Doppler Imaging and Eclipse Mapping have proven to be most effective in detecting starspots on stars exhibiting high levels of magnetic activity, fast rotational velocities, and short rotational periods. Line Depth Ratio has been successfully deployed to calculate surface temperatures of stars similar and dissimilar in type to the Sun, with starspot detection encountering temperature and area accuracy issues.
- The above methodologies have been shown to be capable of detecting instances of stellar variability outside of starspots, including but not limited to, stellar flares, coronal mass ejections, and magnetic dynamo features. Features of stellar variability are common on stars other than the Sun, including starspots and others.
- Further analysis through repeated extensive observations is required to make significant claims about the nature of starspots present on the surface of main sequence stars similar to the Sun.
- There is undeniable scientific overlap between the methodologies presently utilized to detect exoplanets and the procedures taken to detect starspots.
- Future starspot detections will likely require the combined effort and capabilities of those pursuing exoplanet detections and observers documenting heliophysical stellar dynamics.

References

"4 Plasma Interactions." National Research Council. 2004. Plasma Physics of the Local Cosmos. Washington, DC: The National Academies Press. doi: 10.17226/10993.

Albregtsen, F., Joras, P. B., & Maltby, P. (1984). Limb Darkening and Solar Cycle Variation of Sunspot Intensities. \solphys, 90(1), 17–30. doi:10.1007/BF00153781

Apai, D., Rackham, B. V., Giampapa, M. S., Angerhausen, D., Teske, J., Barstow, J., … de Wit, J. (2018). Understanding Stellar Contamination in Exoplanet Transmission Spectra as an Essential Step in Small Planet Characterization. arXiv E-Prints, arXiv:1803.08708. doi:10.48550/arXiv.1803.08708

Araújo, A., & Valio, A. (2021). Kepler-411 Star Activity: Connection between Starspots and Superflares. \apjl, 922(2), L23. doi:10.3847/2041-8213/ac3767

Arlt, R., Vaquero, J.M. Historical sunspot records. Living Rev Sol Phys 17, 1 (2020). https://doi.org/10.1007/s41116-020-0023-y

AURA Space Telescope Science Institute. (2022, July 7). Spectroscopy 101 – Introduction. Webb Space Telescope. Retrieved April 29, 2024, from https://webbtelescope.org/contents/articles/spectroscopy-101--introduction

Blyth, J. (n.d.). The Illustrations of John of Worcester's Chronicle of England (CCC MS 157). Corpus Christi College Oxford. Retrieved April 29, 2024, from https://www.ccc.ox.ac.uk/illustrations-john-worcesters-chronicle-england-ccc-ms-157

Bolles, D. (2024, April 22). How many exoplanets are there? NASA Science. Retrieved April 29, 2024, from https://science.nasa.gov/exoplanets/how-many-exoplanets-are-there

Bolles, D. (2024, January). Heliophysics Big Idea 3.1. NASA Science. Retrieved April 29, 2024, from https://science.nasa.gov/learn/heat/big-ideas/big-idea-3-1/

Bowman, A. (2023, July 25). Understanding the Magnetic Sun. NASA. Retrieved April 29, 2024, from https://www.nasa.gov/science-research/heliophysics/nasa-understanding-the-magnetic-sun/

Bowman, A., & Sabia, S. (2023, November 6). Webb Discovers Methane, Carbon Dioxide in Atmosphere of K2-18 b. NASA. Retrieved April 29, 2024, from https://www.nasa.gov/universe/exoplanets/webb-discovers-methane-carbon-dioxide-in-atmosphere-of-k2-18-b/

Bowman, A., & Sabia, S. (2023, November 6). Webb Discovers Methane, Carbon Dioxide in Atmosphere of K2-18 b. NASA. Retrieved April 29, 2024, from https://www.nasa.gov/universe/exoplanets/webb-discovers-methane-carbon-dioxide-in-atmosphere-of-k2-18-b/

Cameron, A. (2000, September 21). Eclipse movies! St. Andrews Astronomy Group. Retrieved April 29, 2024, from http://star-www.st-and.ac.uk/~acc4/coolpages/movies.html

Cameron, A. C., et al. (2001). Mapping starspots and magnetic fields on cool stars. University of St. Andrews Astronomy Group. Retrieved April 29, 2024, from http://star-www.st-and.ac.uk/~acc4/coolpages/imaging.html

Catalano, S., Biazzo, K., Frasca, A., & Marilli, E. (2002). Measuring starspot temperature from line depth ratios. I. The method. Å, 394, 1009–1021. doi:10.1051/0004-6361:20021223

Center for Astrophysics | Harvard & Smithsonian. (2017, December 15). Starspots | Center for Astrophysics | Harvard & Smithsonian. Harvard CfA. Retrieved April 29, 2024, from https://cfa.harvard.edu/news/starspots

Charbonneau, P., & Wright, O.R. (1995, April 18). The Butterfly Diagram. High Altitude Observatory. Retrieved April 29, 2024, from https://www2.hao.ucar.edu/education/pictorial/butterfly-diagram

Davenport, J. R. A. (2016). The Kepler Catalog of Stellar Flares. \apj, 829(1), 23. doi:10.3847/0004-637X/829/1/23

Hackman, T., Lehtinen, J., Rosén, L., Kochukhov, O., & Käpylä, M. J. (2016). Zeeman-Doppler imaging of active young solar-type stars. Å, 587, A28. doi:10.1051/0004-6361/201527320

Hall, D. (1994). The History of the Discovery of Starspots. International Amateur-Professional Photoelectric Photometry Communications, 54, 1.

Hathaway, D. H. (2017, March 23). NASA/Marshall Solar Physics. NASA/Marshall Solar Physics. Retrieved April 29, 2024, from https://solarscience.msfc.nasa.gov/SunspotCycle.shtml

Hathaway, D. H. (2023, May 3). The Solar Dynamo. NASA/Marshall Solar Physics. Retrieved April 28, 2024, from https://solarscience.msfc.nasa.gov/dynamo.shtml

Helen A. C. Giles, Andrew Collier Cameron, Raphaëlle D. Haywood, A Kepler study of starspot lifetimes with respect to light-curve amplitude and spectral type, Monthly Notices of the Royal Astronomical Society, Volume 472, Issue 2, December 2017, Pages 1618–1627, https://doi.org/10.1093/mnras/stx1931

Howard, W. S., Kowalski, A. F., Flagg, L., MacGregor, M. A., Lim, O., Radica, M., … Dang, L. (2023). Characterizing the Near-infrared Spectra of Flares from TRAPPIST-1 during JWST Transit Spectroscopy Observations. \apj, 959(1), 64. doi:10.3847/1538-4357/acfe75

J L Le Mouël, F Lopes, V Courtillot, Solar turbulence from sunspot records, Monthly Notices of the Royal Astronomical Society, Volume 492, Issue 1, February 2020, Pages 1416–1420, https://doi.org/10.1093/mnras/stz3503

Johansson, E. (n.d.). Wavefront Correction - NSO. National Solar Observatory. Retrieved April 29, 2024, from https://nso.edu/telescopes/dkist/wavefront-correction/

Kochukhov, O. (n.d.). Doppler and Zeeman Doppler Imaging of stellar surfaces. Department of Physics and Astronomy | Uppsala University. Retrieved April 29, 2024, from https://www.astro.uu.se/~oleg/di.html

McCarthy, J. K., Sandiford, B. A., Boyd, D., & Booth, J. (1993). The Sandiford 2.1 M Cassegrain Echelle Spectrograph for McDonald Observatory: Optical and Mechanical Design and Performance. \pasp, 105, 881. doi:10.1086/133250

Medina, A., Winters, J., Irwin, J., & Charbonneau, D. (2021, March). Flare Rates, Rotation Periods, and Spectroscopic Activity Indicators of a Volume-Complete Sample of Mid-to-Late M dwarfs within 15 Parsecs. Bulletin of the American Astronomical Society, 53, 1132.

Monnier, J. (2003). Optical interferometry in astronomy. Reports on Progress in Physics, 66(5), 789-857.

Monnier, J. D., Pedretti, E., Thureau, N., Berger, J.-P., Millan-Gabet, R., ten Brummelaar, T., … Zhao, M. (2006, June). Michigan Infrared Combiner (MIRC): commissioning results at the CHARA Array. In J. D. Monnier, M. Schöller, & W. C. Danchi (Eds.), Advances in Stellar Interferometry (p. 62681P). doi:10.1117/12.671982

Namekata, K., Maehara, H., Notsu, Y., Toriumi, S., Hayakawa, H., Ikuta, K., Notsu, S., Honda, S., Nogami, D., & Shibata, K. (2019). Lifetimes and Emergence/Decay Rates of Star Spots on Solar-type Stars Estimated by Kepler Data in Comparison with Those of Sunspots. \apj, 871(2), 187.

NASA Ames. (2024, April 22). Light Curve of a Planet Transiting Its Star. NASA Science. Retrieved April 29, 2024, from https://science.nasa.gov/resource/light-curve-of-a-planet-transiting-its-star/

National Centers for Environmental Information. (2016, March 30). Sunspot Number Data. National Oceanic and Atmospheric Administration | National Centers for Environmental Information. Retrieved April 29, 2024, from https://www.ngdc.noaa.gov/stp/solar/ssndata.html

National Oceanic and Atmospheric Administration. (2024, January 18). Solar Cycle Progression. Space Weather Prediction Center | National Oceanic and Atmospheric Administration. Retrieved April 29, 2024, from https://www.swpc.noaa.gov/products/solar-cycle-progression

National Oceanic and Atmospheric Administration. (2024, January 19). Sunspots/Solar Cycle. Space Weather Prediction Center. Retrieved April 28, 2024, from https://www.swpc.noaa.gov/phenomena/sunspotssolar-cycle

Neuhäuser R, Arlt R, Richter S. Reconstructed sunspot positions in the Maunder minimum based on the correspondence of Gottfried Kirch. Astron. Nachr. 2018; 339: 219–267. https://doi.org/10.1002/asna.201813481

Orr, K., & Espinoza, L. (2017, April 13). Space Place in a Snap: Where Does the Sun's Energy Come From? Jet Propulsion Laboratory: California Institute of Technology. Retrieved April 29, 2024, from https://www.jpl.nasa.gov/edu/learn/video/space-place-in-a-snap-where-does-the-suns-energy-come-from/

O'Neal, D. (2006). On the Use of Line Depth Ratios to Measure Starspot Properties on Magnetically Active Stars. \apj, 645(1), 659–663. doi:10.1086/504318

Parks, J. R., White, R. J., Baron, F., Monnier, J. D., Kloppenborg, B., Henry, G. W., … Sturmann, L. (2021). Interferometric Imaging of \ensuremath\lambda Andromedae: Evidence of Starspots and Rotation. \apj, 913(1), 54. doi:10.3847/1538-4357/abb670

Pesnell, D., & Patel, A. (n.d.). SDO | Solar Dynamics Observatory. Solar Dynamics Observatory: SDO. Retrieved April 29, 2024, from https://sdo.gsfc.nasa.gov/

Rackham, B. V., Apai, D., & Giampapa, M. S. (2018). The Transit Light Source Effect: False Spectral Features and Incorrect Densities for M-dwarf Transiting Planets. \apj, 853(2), 122. doi:10.3847/1538-4357/aaa08c

Rice, J. B. (2014). General Principles of Doppler Imaging. Brandon University. Retrieved April 29, 2024, from https://people.brandonu.ca/rice/general-principles-of-doppler-imaging/

Rimmele, T.R., Warner, M., Keil, S.L. et al. The Daniel K. Inouye Solar Telescope – Observatory Overview. Sol Phys 295, 172 (2020). https://doi.org/10.1007/s11207-020-01736-7

Roettenbacher, R. M., Monnier, J. D., Korhonen, H., Aarnio, A. N., Baron, F., Che, X., … Sturmann, L. (2016). No Sun-like dynamo on the active star \ensuremath\zeta Andromedae from starspot asymmetry. \nat, 533(7602), 217–220. doi:10.1038/nature17444

Roettenbacher, R. M., Monnier, J. D., Korhonen, H., Harmon, R. O., Baron, F., Hackman, T., … ten Brummelaar, T. A. (2017). Contemporaneous Imaging Comparisons of the Spotted Giant \ensuremath\sigma Geminorum Using Interferometric, Spectroscopic, and Photometric Data. \apj, 849(2), 120. doi:10.3847/1538-4357/aa8ef7

Royal Museums Greenwich. (2023). Sunspots. Royal Museums Greenwich. Retrieved April 29, 2024, from https://www.rmg.co.uk/stories/topics/sunspots

Royal Observatory of Belgium. (2015, July 1). Sunspot Number. Solar Influences Data Analysis Center. Retrieved April 29, 2024, from https://www.sidc.be/SILSO/datafiles

Solar and Heliospheric Observatory. (2020, July 27). SOHO-Gallery, Sunspots. Solar and Heliospheric Observatory. Retrieved April 29, 2024, from https://soho.nascom.nasa.gov/gallery/images/spotcloseinset.html

Solar Dynamics Observatory | NASA. (2024, April 20). Solar images at SDAC. Solar images at SDAC. Retrieved April 29, 2024, from https://umbra.nascom.nasa.gov/images/latest.html

Stanford Solar Group. (2010, July 13). Helioseismic and Magnetic Imager (HMI). Helioseismic and Magnetic Imager for SDO. Retrieved April 29, 2024, from http://hmi.stanford.edu/

StarChild | NASA. (n.d.). What is the solar cycle? StarChild | NASA. Retrieved April 29, 2024, from https://starchild.gsfc.nasa.gov/docs/StarChild/questions/question17.html

Strasbourg astronomical Data Center. (n.d.). CoRoT-2 -- Star. Strasbourg astronomical Data Center. Retrieved April 29, 2024, from https://simbad.u-strasbg.fr/simbad/sim-basic?Ident=GSC+00465-01282

Tran, L., & Thomas, V. (2020, September 15). How Scientists Around the World Track the Solar Cycle. NASA. Retrieved April 29, 2024, from https://www.nasa.gov/science-research/heliophysics/how-scientists-around-the-world-track-the-solar-cycle/

U.S. National Science Foundation. (n.d.). Daniel K. Inouye Solar Telescope - NSO. National Solar Observatory. Retrieved April 29, 2024, from https://nso.edu/telescopes/dki-solar-telescope/

VOGT, S. S., & PENROD, G. D. (1983). DOPPLER IMAGING OF SPOTTED STARS: APPLICATION TO THE RS CANUM VENATICORUM STAR HR 1099. Publications of the Astronomical Society of the Pacific, 95(571), 565–576. http://www.jstor.org/stable/40678209

Walker, E. C. (1944). The Spectrographic Binary, Lambda Andromedae. \jrasc, 38, 249.

Walton, S. R., Preminger, D. G., & Chapman, G. A. (2003). A Statistical Analysis of the Characteristics of Sunspots and Faculae. \solphys, 213(2), 301–317. doi:10.1023/A:1023986901169

Willis, D.M., Wild, M.N. & Warburton, J.S. Re-examination of the Daily Number of Sunspot Groups for the Royal Observatory, Greenwich (1874 – 1885). Sol Phys 291, 2519–2552 (2016). https://doi.org/10.1007/s11207-016-0856-7

Wolter, U., Schmitt, J. H. M. M., Huber, K. F., Czesla, S., Müller, H. M., Guenther, E. W., & Hatzes, A. P. (2009). Transit mapping of a starspot on CoRoT-2. Probing a stellar surface with planetary transits. Å, 504(2), 561–564. doi:10.1051/0004-6361/200912329